# Local earthquake tomography of central Costa Rica: transition from seamount to ridge subduction

A. Nilay Dinc,[1,*] Ivan Koulakov,[2] Martin Thorwart,[1] Wolfgang Rabbel,[1] Ernst R. Flueh,[3] Ivonne Arroyo,[3] Waldo Taylor[4] and Guillermo Alvarado[4]

[1] *Institute of Geosciences*, SFB574, *Christian-Albrechts-University, Otto-Hahn-Platz*1, 24118, *Kiel, Germany. E-mail: aysun.n.dinc@exxonmobil.com*
[2] *Institute of Petroleum Geology and Geophysics, SB RAS, Prospekt Akademika Koptuga*, 3, *Novosibirsk* 630090, *Russia*
[3] *IFM-GEOMAR, Wischhofstr.* 1-3, 24108, *Kiel, Germany*
[4] *Área de Amenazas y Auscultación Sísmica y Volcánica, Instituto Costarricense de Electricidad, Apdo* 100032, *San José, Costa Rica*

GJI Seismology

**SUMMARY**

The structure and seismicity of the subduction zone of central Costa Rica have been investigated with local earthquake tomography down to *ca.* 50 km depth. Seismic traveltime data sets of three on- and offshore seismic networks were combined for a simultaneous inversion of hypocentre locations, 3-D structure of *P*-wave velocity and $V_p/V_s$ ratio using about 2000 high-quality events. The seismicity and slab geometry as well as $V_p$ and $V_p/V_s$ show significant lateral variation along the subduction zone corresponding to the changes of the incoming plate which consists of serpentinized oceanic lithosphere in the northwest, a seamount province in the centre and the subducting Cocos Ridge in the southeast of the investigation area. Three prominent features can be identified in the $V_p$ and $V_p/V_s$ tomograms: a high-velocity zone with a perturbation of 4–10 per cent representing the subducting slab, a low-velocity zone (10–20 per cent) in the forearc crust probably caused by deformation, fluid release and hydration and a low-velocity zone below the volcanic arc related to upwelling fluids and magma. Unlike previously suggested, the dip of the subducting slab does not decrease to the south. Instead, an average steepening of the plate interface from 30° to 45° is observed from north to south and a transition from a plane to a step-shaped plate interface. This is connected with a change in the deformation style of the overriding plate where roughly planar, partly conjugated, clusters of seismicity of regionally varying dip are observed. It can be shown that the central Costa Rica Deformation Belt represents a deep crustal transition zone extending from the surface down to 40 km depth. This transition zone indicates the lateral termination of the active part of the volcanic chain and seems to be related to the changing structure of the incoming plate as well.

**Key words:** Seismicity and tectonics; Seismic tomography; Subduction zone processes.

## 1 INTRODUCTION

The Central America convergent margin of Costa Rica has been intensively studied for many years because strong lateral variations in the subduction system (in coming plate, seismicity, arc volcanism) are encountered at relatively short distances, making this an ideal laboratory to investigate subduction zone processes. Lateral changes along the volcanic arc of the overriding Caribbean Plate have been understood as a consequence of lateral changes in the structure, age and composition of the incoming oceanic Cocos Plate (Fig. 1) (Werner *et al.* 1999; Barckhausen *et al.* 2001; Carr *et al.* 2007; Hoernle & Hauff 2007). The incoming plate has been divided

into three segments (Fig. 2) based on their morphology (von Huene 1995), which are as follows:

(1) A rather smooth segment of regular oceanic lithosphere with long trench parallel fractures of northern Costa Rica (Nicoya Peninsula segment) continuing to Nicaragua,

(2) a topographically rough segment covered with seamounts of central Costa Rica (Jaco-Quepos segment) and

(3) the thickened and rough oceanic lithosphere of the Cocos Ridge (Walther 2003) subducting beneath southern Costa Rica (Osa Peninsula segment).

A corresponding segmentation is found along the arc of the overriding plate: it is volcanically active along the projection of sections 1 and 2 but shows major geochemical differences in the magmas between 1 and 2 (Carr *et al.* 2003). Above the subducting Cocos

*Now at: ExxonMobil Exploration Company, 222 Benmar Dr. Houston, TX 77060, USA.
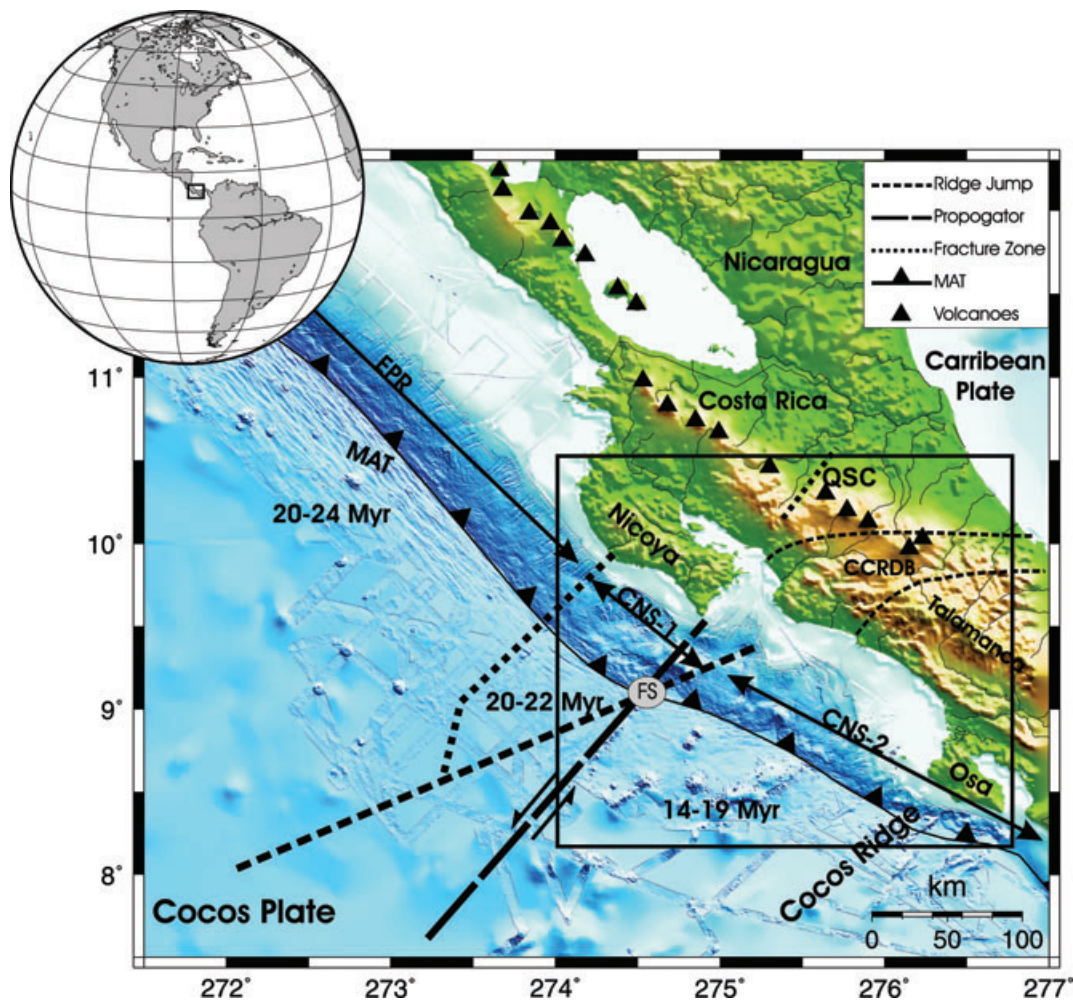
**Figure 1.** Tectonic settings of Costa Rica and Nicaragua. Offshore tectonic structures are from Barckhausen *et al.* (2001). MAT: Mid-America Trench; EPR: East Pacific Rise; CNS-1: Cocos Nazca Spreading Centre 1; CNS-2: Cocos Nazca Spreading Centre 2; FS: Fisher Seamount. Onshore tectonic structures are from Walther *et al.* (2000) and Protti *et al.* (1994). CCRDB: Central Costa Rica Deformation Belt; QSC: Quesada Sharp Contortion. The rectangular box indicates the study area. For a more detailed view see Fig. 2.

Ridge, the Talamanca mountain range formed where the active volcanism stopped in the Late Miocene (Graefe 1998). The Talamanca shows a recent uplift rate of up to 4.7 mm yr$^{-1}$ as observed along the coast of Osa Peninsula (Gardner *et al.* 1992).

The investigation area is located in central Costa Rica and extends from the trench to the volcanic front (Fig. 2). It thus covers the forearc area of the seamount subduction province as well as its border to the Osa segment. By applying joint on- and offshore local earthquake tomography, we investigate the following points related to the question of stress transfer and mass transport from the subducting to the overriding plate.

(i) Do the seismogenic zone and stress transfer change in correspondence to the incoming plate?

(ii) If so, what changes in slab geometry and are crustal structures related to these variations?

(iii) Is there evidence of fluid transport from the dewatering subducting plate into the mantle wedge and up to the volcanic arc?

(iv) Do the seismic velocities or $V_p/V_s$ ratio indicate substantial differences in the crustal structure across the edge of the active section of the volcanic arc?

Based on two seismic networks with an average station spacing of ~15 km, we aimed to obtain high-resolution *P*- and *S*-wave tomo-

graphic images and hypocentre locations as a basis for tectonic interpretation. Previous local seismicity and teleseismic studies based on the Costa Rican permanent regional network were performed with *P* waves only. They cover the central part of Costa Rica almost completely but with a lower spatial resolution and they do not include the offshore area (Colombo *et al.* 1997; Protti *et al.* 1999; Yao *et al.* 1999; Sallares *et al.* 2000; Quintero & Kissling 2001; Husen *et al.* 2003). A detailed tomographic view of the northwestern part of our study area has been presented recently by Arroyo *et al.* (2009) based on a subset of the data of this study. Whereas Arroyo *et al.* (2009) focus on the local structure of the subducting slab, our study intends to investigate lateral changes along the subduction zone on a larger scale. Further geophysical and geologic background information is provided by regional studies including seafloor age dating (Barckhausen *et al.* 2001; Hoernle & Hauff 2007) and a wealth of geological, tectonic and volcanological investigations (for an overview see, e.g. Bundschuh & Alvarado 2007).

Our paper is organized as follows: the relevant geological and geophysical background information are summarized in Section 2. The data basis comprising data from two independently recorded networks (JACO and QUEPOS) and the tomographic algorithm are described in Section 3. Resolution tests to demonstrate the reliability
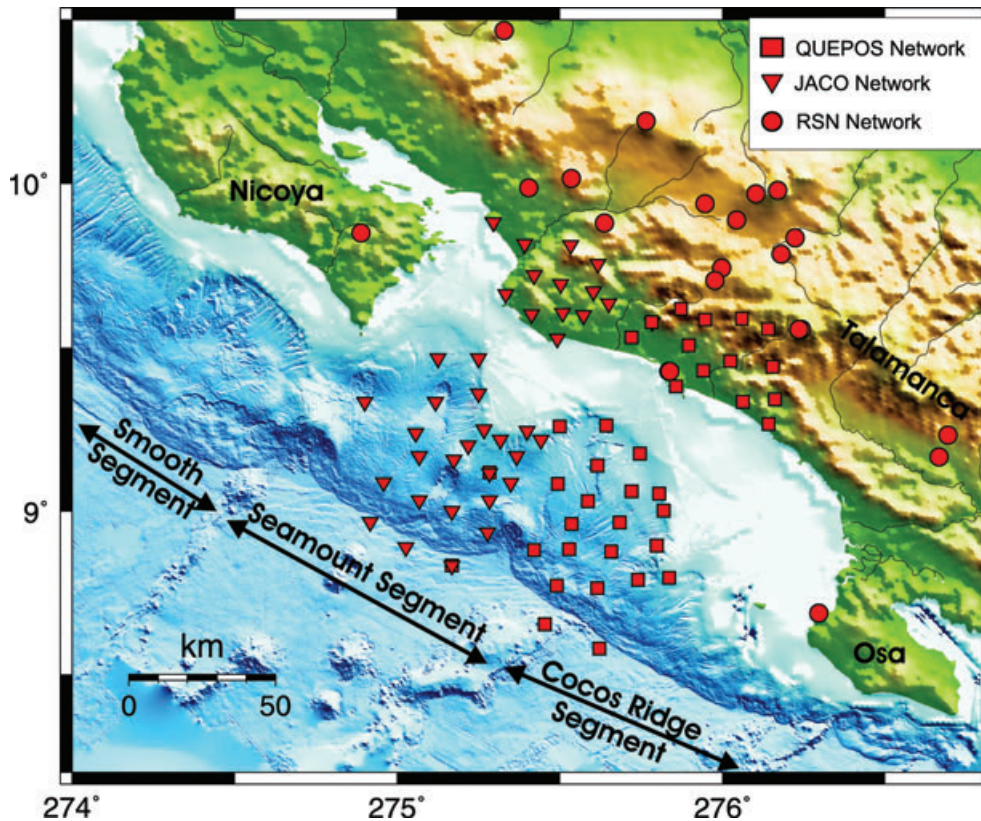
**Figure 2.** Tectonic segments and station distributions in central Costa Rica.

of the results are described in Section 4. Results, discussions and conclusions are given in Sections 5 and 6, respectively.

## 2  GEOLOGY AND TECTONIC SETTINGS

The composition and the segmentation of the Cocos Plate have been defined by magnetic anomalies (Barckhausen *et al.* 2001), multibeam bathymetry (von Huene 1995; von Huene *et al.* 2000), seismic studies (Walther & Flueh 2002; Sallares & Charvis 2003; Walther 2003; Wilson *et al.* 2003; Sallares *et al.* 2005) and geological sampling (Hauff *et al.* 1997; Werner *et al.* 1999; Wilson *et al.* 2003; Hoernle & Hauff 2007). Following these studies, the Cocos Plate is generated at two different zones, the East Pacific Rise (EPR) in the west and the Cocos-Nazca Spreading Center (CNS) in the south. The part of the Cocos Plate generated along the EPR subducts beneath Nicaragua and northern Costa Rica. At the trench it is 20–24 Myr old. The part of the Cocos Plate generated at the CNS-1 is 20–22 Myr old where subducting beneath northern Costa Rica (Nicoya), and 14–19 Myr old (CNS-2) where subducting under southern Costa Rica (Fig. 1).

Numerous seismic marine multichannel reflection and onshore–offshore wide-angle refraction surveys have been carried out in the past decade to characterize the Pacific Costa Rican margin (Hinz *et al.* 1996; Ye *et al.* 1996; Flueh & von Huene 2007). These studies show that the margin is currently eroding. The top of the wedge has only a thin sedimentary cover and is composed of oceanic crust similar to the ophiolitic outcrops found along the Costa Rican coast. The plate boundary is highly reflective along the whole Costa Rican margin. Seismic wide-angle studies suggest the presence of a thin low-velocity layer of subducted sediment

along the plate boundary. Offshore, close to the shoreline, the plate boundary is generally found at 12–15 km depth. The dip of the plate boundary is decreasing from northwest (NW) to southeast (SE), and the margin wedge is thinnest in central Costa Rica where numerous seamounts are subducted.

This observation is also in agreement with seismological investigations, showing that the dip of the seismogenic zone and the Wadati Benioff Zone (WBZ) seismicity is decreasing from Nicaragua to southern Costa Rica. Also the maximum depth of the WBZ seismicity decreases from 200 km in Nicaragua to 80 km in southern Costa Rica (Protti *et al.* 1995). Central Costa Rica is characterized by a higher seismicity compared to northern Costa Rica (Nicoya Peninsula) and southern Costa Rica (Osa Peninsula). However, large events with magnitudes >7 are only known from the Nicoya and the Osa segments, whereas in central Costa Rica no historical earthquake larger than magnitude 7.0 has been recorded. This suggests weaker seismic coupling in central Costa Rica, perhaps as a consequence of seamount subduction (Protti *et al.* 1994, 1995).

Most of our knowledge about Costa Rican seismicity results from the regional networks in Costa Rica, which have been operated since the early1980s. Sallares *et al.* (2000) and Quintero & Kissling (2001) compiled these data and presented a *P*-wave velocity model for Costa Rica. Their model shows that the average velocity is generally low and does not exceed 8.0 km s$^{-1}$ in the upper 50 km of the mantle. In their study, the accuracy of hypocentre determination is limited by the application of a 1-D seismic velocity model and, more importantly, the lack of stations in the offshore area where most of the seismogenic zone earthquakes occur. Husen *et al.* (2002, 2003) used this data set for a tomographic 3-D inversion, and demonstrated the complexity and large lateral variability of the crustal and lithospheric structure. They find an evidence for a

subducted seamounts at 30 km depth beneath the shoreline (Husen *et al.* 2002). However, the seismogenic zone is not well resolved because of an unfavourable ray geometry of offshore earthquakes and onshore stations.

The seismogenic zone was investigated in more detail using local amphibious networks near Osa Peninsula (DeShon *et al.* 2003) and of Nicoya Peninsula (Newman *et al.* 2002; DeShon *et al.* 2006). These data enabled to distinguish plate interface earthquakes from intraplate earthquakes. The authors also found evidence for mantle wedge serpentinization. Based on onshore GPS data also locked and free slip areas of the seismogenic zone could be defined (Norabuena *et al.* 2004). Geographically, the data presented in our study form a bridge between these previous Nicoya and Osa seismic networks.

## 3 DATA BASE AND INVERSION ALGORTIHM

Two temporary amphibious seismological networks, named JACO and QUEPOS, were deployed along the Pacific coast of central Costa Rica in 2002 and 2003, respectively. The networks comprised a total of 46 ocean bottom and 27 land stations (Fig. 2). Most of the marine stations were only hydrophones, 10 of them were equipped with seismometers [IFM-Geomar type OBS as described by Bialas & Flueh (1999)]. The land stations were short period Mark-L-3D seismometers with Reftek recorders provided by the German instrument pool of GFZ (Potsdam). JACO was operated from April 2002 to October 2002 while QUEPOS was operated from September 2002 to May 2003.

During the picking procedure three classes were assigned for the observational weights: impulsive, emergent and questionable. The corresponding uncertainties are defined as $\pm 0.05$ s for impulsive, $\pm 0.1$ s for emergent and $>0.2$ s for questionable observational weights.

More than 8000 earthquakes were located by the standard earthquake location procedure HYPO77 applying the optimum 1-D model (Table 1) for the Costa Rica region which was initially taken from Quintero & Kissling (2001) and then revised using the VELEST code for 1-D model optimization (Kissling *et al.* 1994). In addition, we have performed the inversions for several different starting models. The tomographic results were stable with respect to variations of the initial background velocity model.

**Table 1.** Background model of $V_p$ and $V_s$ applied in the tomographic inversion.

| Depth (km) | $V_p$ (km s$^{-1}$) | $V_s$ (km s$^{-1}$) |
|---|---|---|
| 0.0 | 4.45 | 2.50 |
| 4.0 | 5.50 | 3.00 |
| 6.0 | 5.60 | 3.15 |
| 8.0 | 6.00 | 3.37 |
| 11.0 | 6.15 | 3.45 |
| 14.0 | 6.25 | 3.51 |
| 21.0 | 6.50 | 3.65 |
| 28.0 | 6.80 | 3.82 |
| 34.0 | 7.00 | 3.93 |
| 44.0 | 7.30 | 4.10 |
| 54.0 | 7.90 | 4.44 |
| 74.0 | 8.20 | 4.60 |
| 104.0 | 8.30 | 4.66 |
| 124.0 | 8.35 | 4.69 |
| 154.0 | 8.40 | 4.72 |
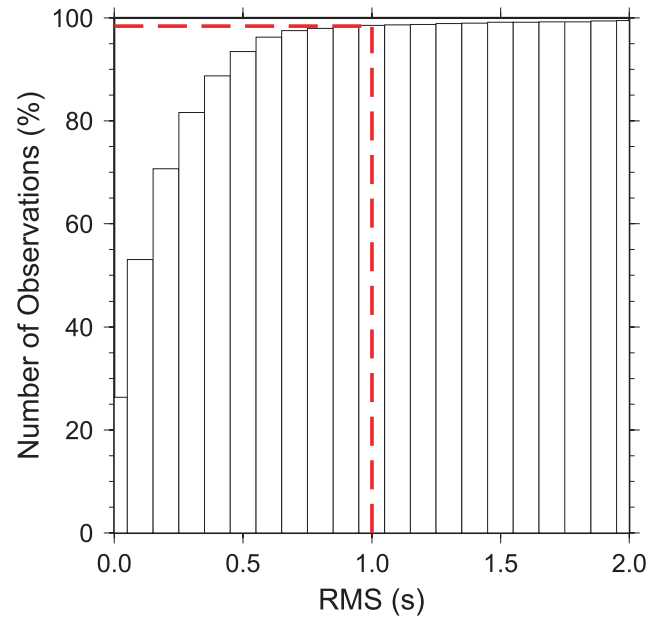
**Figure 3.** Cumulative RMS distribution of the events. Note that only 2 per cent of the events show RMS higher than 1 s.

*P* wave onsets recorded by the stations of the Red Sismolgica Nacional of Costa Rica (RSN) were also included into the database to improve the coverage and to increase the number of intraplate and WBZ events. The cumulative RMS distribution of these events (Fig. 3) show that 98 per cent of the data set has the RMS smaller than 1 s.

For the tomographic inversion, the data set was edited on the basis of a preliminary hypocentre localization with a 1-D velocity model and of the following criteria:

(1) each event observed at a minimum of 10 P picks for *P*-wave inversion and a minimum of 10 P and 5 S picks for $V_p/V_s$ inversion;

(2) horizontal distance to the nearest station of the network $<150$ km;

(3) rejection if traveltime residual after preliminary localization $>1$ s;

(4) elimination of events which show deviations larger than 2 km in the horizontal and less than 5 km in the vertical position which is determined by a statistical approach described in the following paragraph.

Applying these criteria, 31 912 *P*-wave and 9298 *S*-wave traveltime observations from 2079 events were selected for the inversion (Fig. 10).

A comparative test showed that the application of criterion (3) had only a negligible influence on the results, probably because only 2 per cent of the data were affected by criterion (3) (Fig. 3).

We did not apply the GAP criterion used in most local earthquake tomography studies, which takes into consideration only events located inside the network perimeter. First, in our catalogue we do not have many out-of-network events (GAP < 220 deg). Secondly, it was shown by Koulakov (2009b) that such events can be of great use for improving the resolution of the inversion.

In the catalogue used for tomographic inversion, most of the *S* picks correspond to the onshore stations, because most of offshore stations were equipped by hydrophones that cannot be used for picking the *S* phases. Therefore, the resolved area for the *S* velocity model covers mostly the onshore part of the study area.
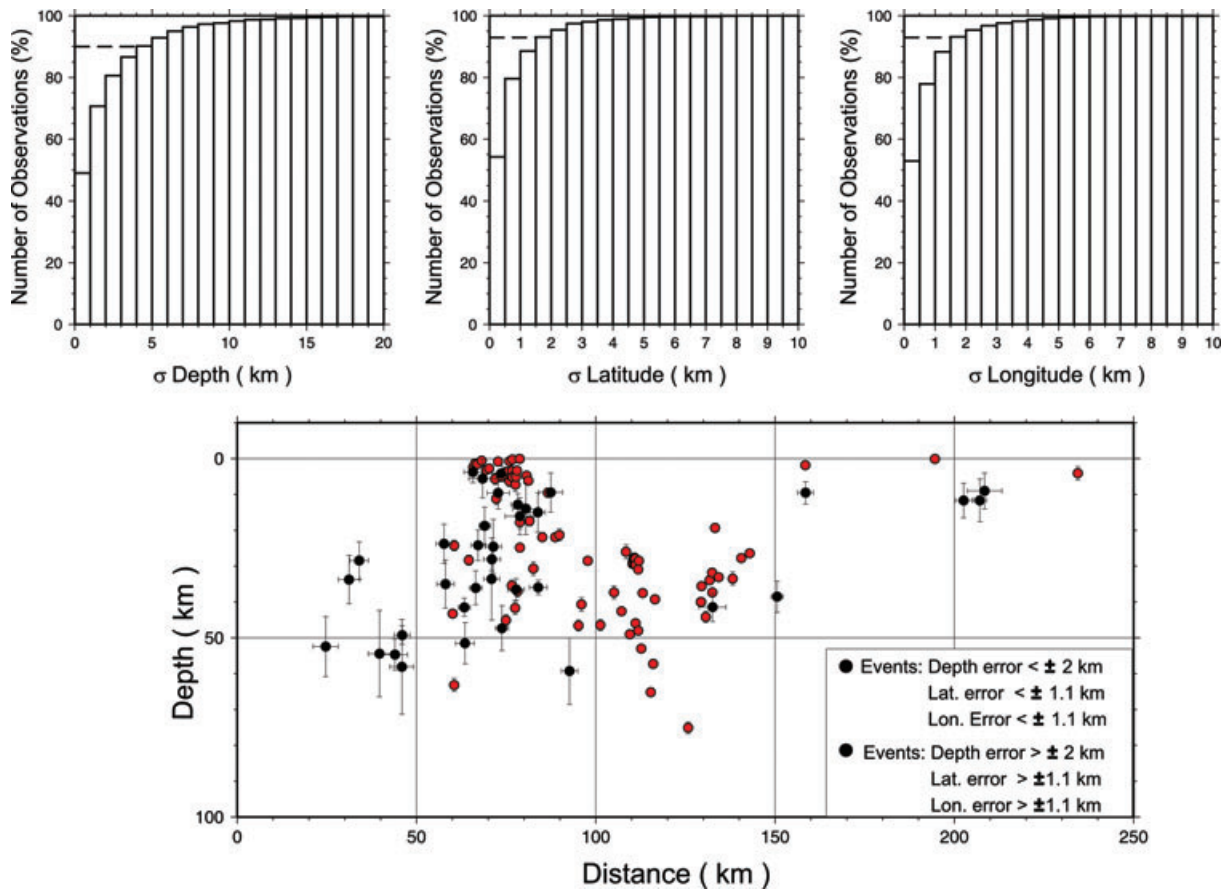
**Figure 4.** Statistical approach for calculating the standard deviation of events in the mean of latitude, longitude and depth. Upper row shows the histograms indicating the distribution of deviations for all events. Lower row is the distribution of events in a depth–distance section along profile-6 in Fig. 10. Red circles indicate the events with small deviations which are selected for the data base and black circles denote the rejected events.

To estimate the uncertainty of the hypocentre locations, required for criteria (4), the following approach was applied: We randomly selected 10 subsets of the original data set containing 70 per cent of the data. Each subset was inverted in five iterative steps using the same inversion procedure [LOTOS code (Koulakov 2009a) described in the next paragraphs] and same parameters as applied to the full data set. After the inversion, the deviations of the hypocentre locations and velocity models were calculated with respect to the average value and visualized in form of accumulative frequency distribution for the hypocentre locations. By picking the 95 per cent limits from Fig. 4, we estimated global standard deviations of 2 km and 5 km for the horizontal and vertical coordinates of the hypocentres, respectively. For the subsequent final tomographic inversion, we edited the traveltime data again keeping only those events in the data base which had shown deviations less than 2 km in horizontal and less than 5 km in vertical position, reducing the number of events from 3044 to 2079. The same procedure provided the uncertainty estimates for the velocity perturbations shown in the form of horizontal sections (Fig. 5). In the figures of the final results (Figs 11–15), the velocity fields with a standard deviation higher than 5 per cent were not visualized.

The 3-D seismic velocity structure, hypocentre locations and station corrections are calculated iteratively and simultaneously by using the LOTOS code (LOcal TOmography Software) by Koulakov *et al.* (2007) and Koulakov (2009a). The processing starts with preliminary source locations in the 1-D velocity model estimated based on the VELEST code (Kissling *et al.* 1994). The location procedure

at this preliminary step is based on using a previously computed table of reference times that allows speeding up the calculations.

The non-linear tomographic inversion is performed in several iterations, which consist of the following steps.

(1) *Locating the sources using the 3-D velocity model*. The algorithm updates the coordinates of a source using a gradient method. The rays in a 3-D velocity model are computed using the bending method using the basic idea proposed by Um & Thurber (1987).

(2) *Parameterization*. Here we use the parameterization with nodes that are installed according to the distribution of rays in the 1-D model. The spacing of the grid is kept considerably smaller than the expected minimal size of the resolved anomalies. Moreover, to further decrease the influence of the parameterization on the results, the inversion is repeated using several grids configurations with different basic orientations (e.g. 0°, 22°, 45° and 66°). The results obtained for these grids are combined in to one model by simple averaging.

(3) The inversion was performed simultaneously for *P* and *S* velocity anomalies with respect to the model derived in the previous iteration and for the source parameters. Alternatively, in this study the inversion was also carried out for $V_p$ and $V_p/V_s$ ratio using the algorithm described in (Koulakov *et al.* 2007). The inverted velocity anomalies are damped by using two additional matrix blocks, which control amplitude and smoothing of the solution. The sparse matrix is inverted using the LSQR algorithm (Paige & Saunders 1982; van der Sluis & van der Vorst 1987). The damping parameters
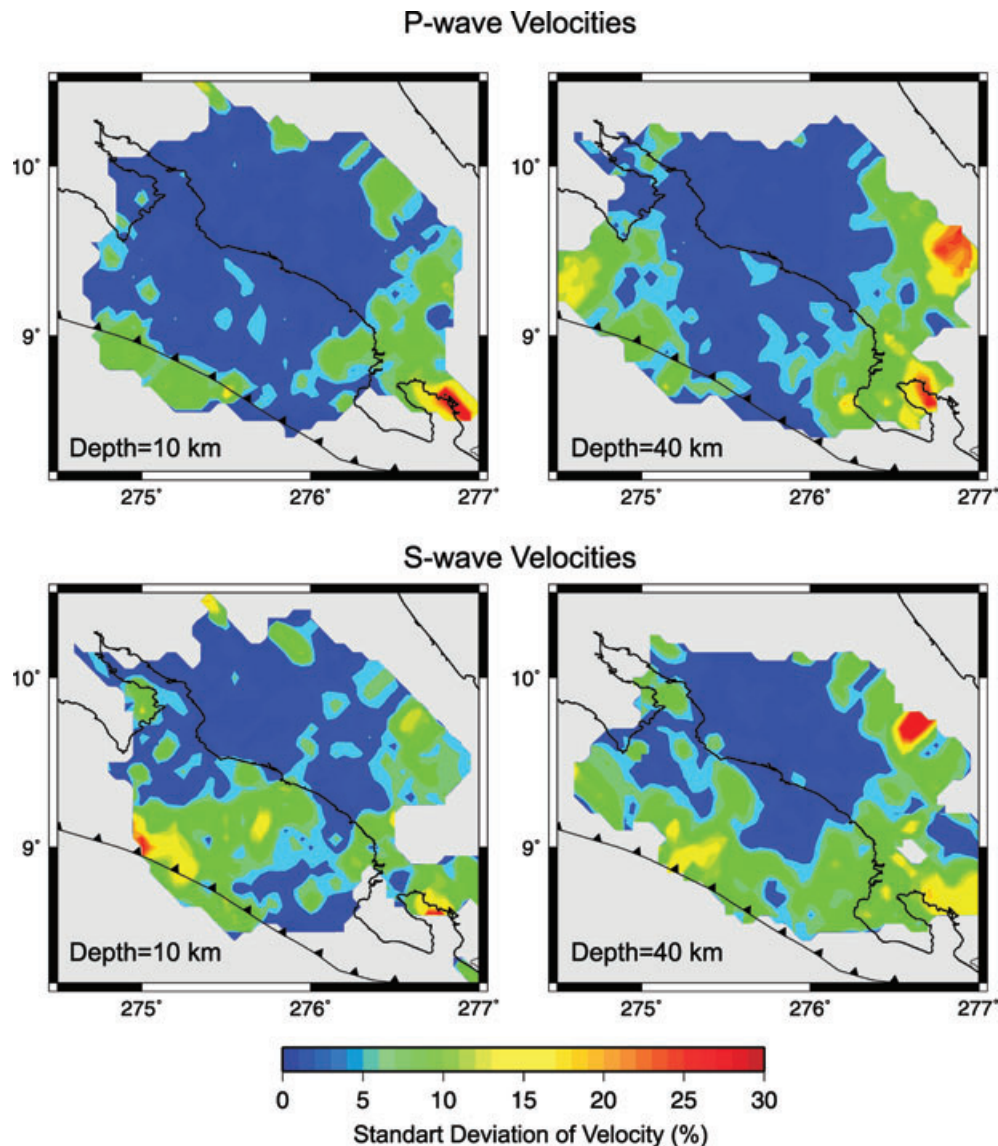
**Figure 5.** Statistical approach for calculating the standard deviation of the velocity perturbations at each grid node based on 10 randomly selected subsets of traveltime data. Upper row is for the *P*-wave perturbations: 75 per cent of the grid nodes had a standard deviation smaller than 5 per cent. Lower row is for the *S*-wave perturbations: 70 per cent of the grid nodes had a standard deviation smaller than 5 per cent.

were evaluated after the inversion of the synthetic data sets. The values of the free parameters were optimized by maximizing the similarity between the initial model, both in terms of amplitude and the positions of the synthetic patterns.

(4) The models derived using different grids are then averaged and combined to provide a 3-D model of absolute *P* and *S* velocities. This model is then used as a basic one for the next iteration which consists of the steps (1), (3) and (4). In total, we used five iterations of the tomographic cycle.

# 4  RESOLUTION TESTS

To show that the tomographic inversion produces reliable images of the subsurface structure, we investigated the stability of inversion results with respect to a random selection of input data and performed two different tests of spatial resolution based on synthetic data. Because the data are combinations of three different networks

operated in different time periods, we paid special attention to the resolution in the overlapping areas.

## 4.1  Test with a random selection of events

To investigate the influence of random noise in the real traveltime data, we performed independent inversions for two randomly separated data subsets. The subsets were selected by choosing events with either odd or even identification numbers. In the case of a strong noise influence, the correlation between the different results should be low. In Fig. 6, results are presented in two vertical and one horizontal sections corresponding to the independent inversion of data sets with odd, even and all events. It is obvious that the prominent features are recognizable in all subsets. Even small patterns in the coastal area are robustly retrieved with both data subsets. The test shows that the noise in the data has negligible effect on the stability of the results.
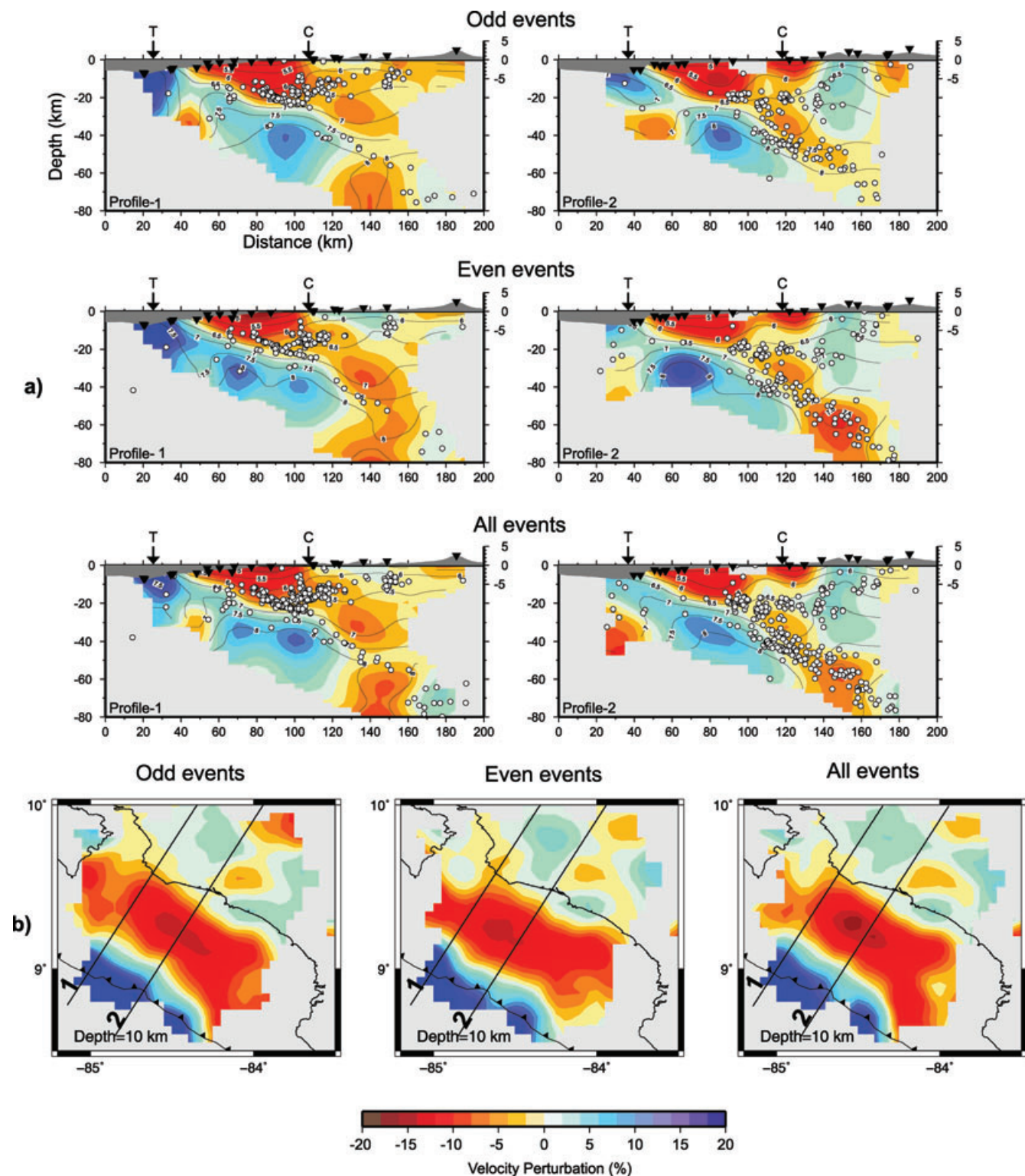
**Figure 6.** *P* velocity anomalies obtained from the inversion of odd, even number of events and all data set. (a) Vertical sections along the profiles 1 and 2 shown in Fig. (b). White circles: earthquakes; T: trench; C: coast; triangles: stations. Contours represent the absolute velocities with an interval of 0.5 km s$^{-1}$. (b) Horizontal sections from 10 km depth. The shape and the amplitude of the high velocity slab (blue), low velocity forearc (red) and the overriding plate structures are similarly reconstructed after the inversions with three different data set; odd, even number of events and all data set, respectively.

### 4.2 Tests with synthetic data

To check the spatial resolution of the actual data set, we performed three different tests with synthetic data. In each test, the synthetic traveltimes were computed by 3-D ray tracing through a synthetic model using the actual configuration of sources and receivers. To simulate real conditions, we added random noise to the traveltimes with 0.2 s standard deviation similar to the real traveltime residuals
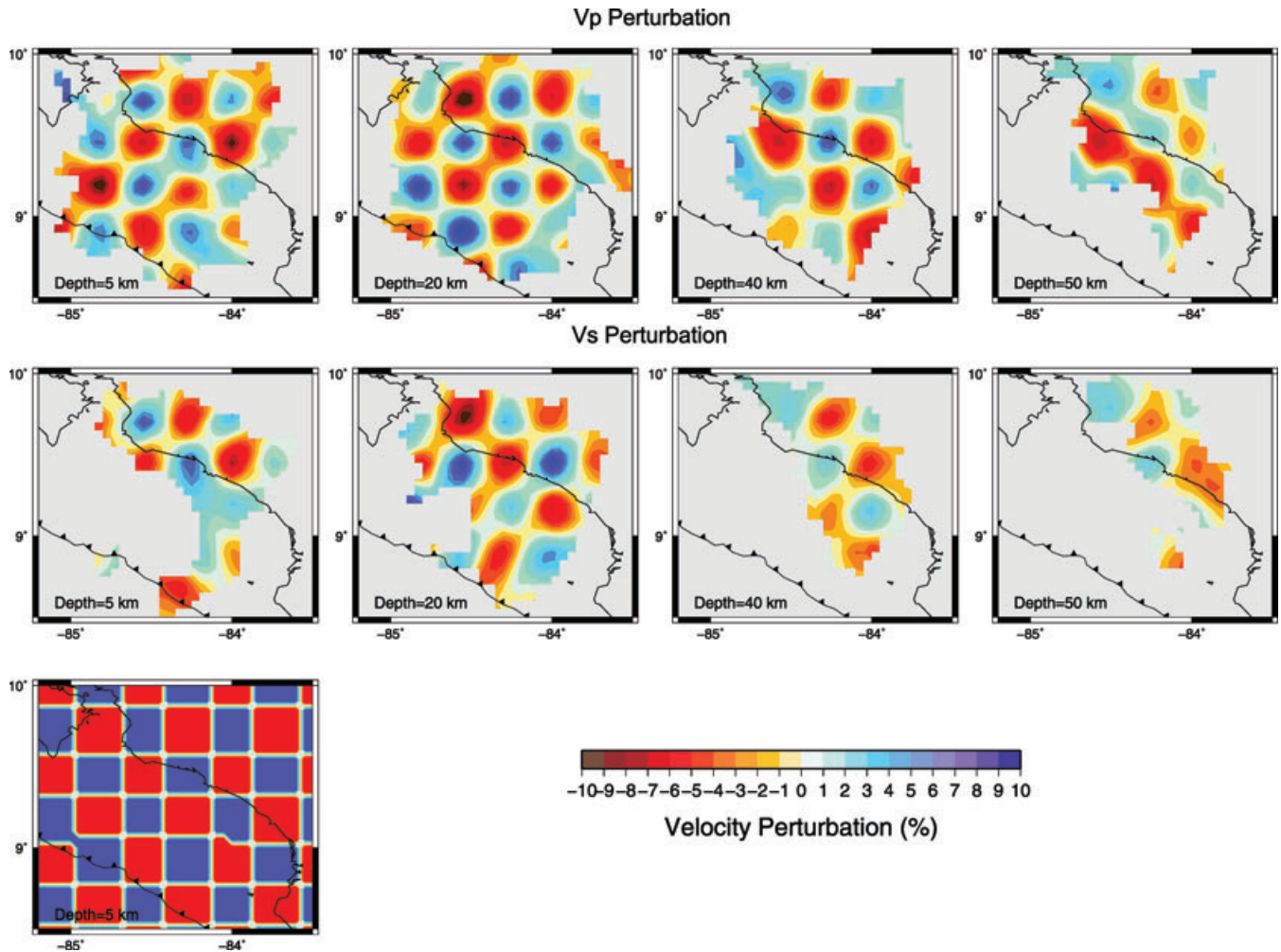
**Figure 7.** A checkerboard sensitivity test was performed to evaluate the resolution capability of the data set and sensitivity of the model. The velocities of the initial model were modified by an amplitude of ±7 per cent of the initial 1-D velocity model (Table 1), alternating in both horizontal and vertical directions with a grid size of 30 × 30 × 20 km (lower left corner). The synthetic traveltimes were calculated for this model and distorted using randomly distributed noise with 0.2 s RMS for both *P* and *S* data. Upper row shows the reconstructed model for $V_p$ and the middle row shows the reconstructed model for $V_s$.

after the final inversion. The reconstruction was performed using the same program codes and parameters as in the real case: We started with source localization accepting that the sources would be shifted from the 'true' positions. After several iterations, the algorithm shifted the sources close to their initial position and retrieved the velocity model.

### 4.2.1 Checkerboard test

To check the horizontal and vertical resolution, we performed a checkerboard test. The initial configuration is presented in Fig. 7 (lower row). The block size is 30 × 30 × 20 km. The anomalies represent alternating high- and low-velocity blocks of ±7 per cent amplitude of the initial velocity model (Table 1). The alternation is set up in both horizontal and vertical directions. In Fig. 7, we show the reconstruction results for *P*- and *S*-wave velocity models at depth levels of 5, 20, 40 and 50 km. It can be seen that the *P*-wave velocity anomalies are well reconstructed in shape and amplitude beneath the entire study area. Up to the depth of 30 km, the resolution is also good for the *S*-wave model. However, at deeper levels, the resolution is lower for the *S* waves due to the smaller

number of data and subsequently poor ray coverage in the offshore part.

### 4.2.2 Resolution of realistic velocity anomaly

The aim of the second test was to check how well the amplitudes of realistic velocity anomalies would be reproduced for a synthetic velocity model showing a similar subsurface structure as the Costa Rica subduction zone (Fig. 8 top, compare with Fig. 11, Profile-2). The tomographic image (Fig. 8 bottom) reproduces shape and amplitude of the true model well. However, maximum reconstructed velocity amplitudes are about 2 per cent smaller than the amplitudes of the true model.

## 5 RESULTS OF TOMOGRAPHIC INVERSION

The tomographic inversion procedure was applied to the combined JACO, QUEPOS and RSN data sets. The 3-D inversion was terminated after five iterations. RMS traveltime residuals were reduced from 0.31 to 0.13 s for *P*-wave data and from 0.33 to 0.14 s for
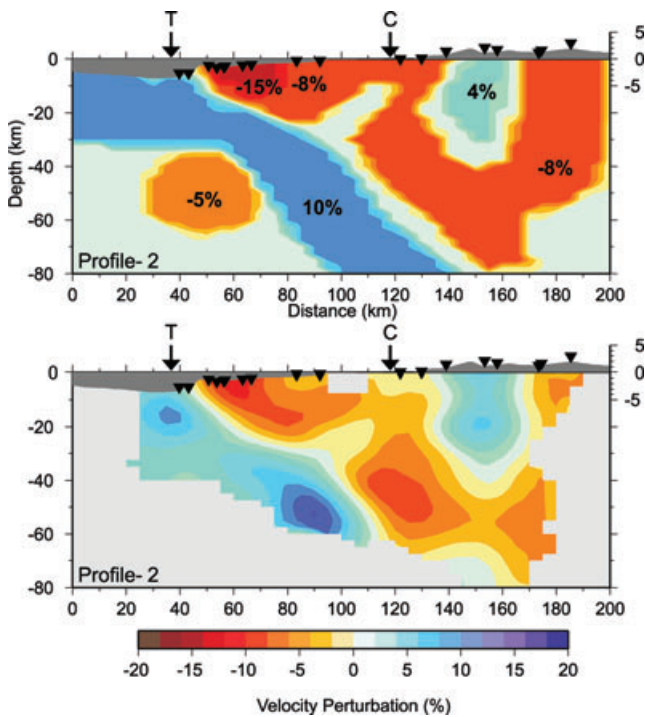
**Figure 8.** Synthetic test to check the vertical resolution with real anomalies. The upper row is the synthetic model along profile-2 (Fig. 11) showing the defined perturbations in percentage. The last row is the recovered model. The noise of 0.2 s RMS was added to the synthetic traveltimes. The result of reconstruction is identical with the real inversion case and reproduces the main patterns. T: trench and C: coast and triangles indicate the stations.

**Table 2.** Reduction of traveltime residuals during five iterations of inversion procedure.

|  | 1. Iteration | 2. Iteration | 3. Iteration | 4. Iteration | 5. Iteration |
|---|---|---|---|---|---|
| *P*-RMS (s) | 0.31 | 0.17 | 0.14 | 0.13 | 0.127 |
| *S*-RMS (s) | 0.33 | 0.18 | 0.15 | 0.14 | 0.137 |

*S*-wave data (Table 2). This corresponds to a variance reduction of 60 per cent for *P*- and *S*-wave traveltime residuals with respect to the 1-D starting model.

To check possible systematic errors, such as mislocation of stations and timing problems, the distribution of the *P* and *S* traveltime residuals for each station is presented in Fig. 9. The average residuals distributed between ±0.1 s for the stations with higher number of phase readings. The stations with a smaller number of picked arrivals show larger residuals. However, because of the small number of picks, they do not contribute to the inversion significantly. A systematic residual trend has not been observed.

The tomographic results are presented in the form of vertical depth sections (Figs 11–13) and horizontal depth slices (Fig. 15). The vertical sections are arranged along profiles perpendicular and parallel to the trench (Fig. 10). The figures show *P*-wave velocity perturbations (Fig. 11) relative to the 1-D reference model (Table 1), absolute *P*-wave velocities (Fig. 12) and $V_p/V_s$ ratios (Fig. 13). Velocity perturbations are mostly used for interpretation because variations of the physical state of the materials are more easily seen. Hypocentres within a ±10 km wide band are projected onto the vertical sections.

## 5.1 Seismicity

The seismicity observed in the vertical sections (Figs 11–13) can be classified in four groups. Specific clusters of seismicity are indicated in Figs 12 and 13 and redrawn with index numbers in Fig. 14. These fault drawings are intended to highlight the trends and line-ups visible in the seismicity patterns and their changes from N to S. Note that they do not necessarily represent individual single faults.

(i) Interplate seismicity at crustal levels occurs between 10 and 30 km depths at 35 and 90 km distance from the trench. Enhanced earthquake clustering is found in the northern profiles 1 and 2 at about 20 km depth where the plate interface bends from 20° to 30° dip (point B and cluster 1a; Fig. 14). Further to the south, in profiles 3 and 4, the clustering is significantly weaker. A special situation is found along profiles 6 and 7 where near-surface interplate seismicity is weak but a dense pattern of linearly aligned events extends within the forearc from the surface down to 20 km depth (cluster EQ in Fig. 14). This pattern represents the aftershocks of the $M = 6.9$ earthquake of 1999 August 20 (Rafael & Alvaro 1999). It starts at the bending point of the plate interface at 20 km depth and lines up to the surface with 40° dip in straight prolongation of the deeper plate interface. Interplate events are found closer to the trench (cluster 1b in Fig. 14) where they line up more steeply than in the north according to the more complicated plate geometry.

(ii) At the forearc mantle level, the Wadati–Benioff Zone can be followed in the whole area of the network down to a depth of 80 km and up to maximum distances of 110–150 km from the trench (clusters 2a and b in Fig. 14). At about 20 km depth, all sections show a bending point of the plate interface below which the dip remains constant (B in Fig. 14). Laterally, however, the dip angle of the WBZ seismicity increases from 30° in the north to 45° in the south (profiles 1–6 in Fig. 11) showing an abrupt change between profiles 4 and 5. Generally, the density of seismic events observed in the WBZ is lower in northwestern than in southeastern Costa Rica.

(iii) Within the overriding plate seismicity appears in zones of aligned events connecting the WBZ to the volcanic arc. Along the northern profiles 1–3 (Fig. 12), these linear clusters seem to form 20°S dipping parallel fault planes extending from a depths of 20–30 km up into the forearc and to the volcanic chain at the surface (cluster 3a in Fig. 14). Along the southern profiles 5 and 6, the seismicity cluster form criss-cross lineaments of 35° dip which could be interpreted as conjugate thrust planes (cluster 3b in Fig. 14). This type of seismicity starts near the WBZ at a depth of 40–50 km and extends obliquely towards the Talamanca range. Along profiles 3 and 4, which cover the transition from the active volcanic chain to the presently volcanically inactive Talamanca range, patterns 3a and 3b in Fig. 14 seem to interfere.

(iv) Seismicity within the subducting plate was found on sections 5 and 6 (Fig. 12) in a linear cluster extending from the plate interface into the subducting plate (cluster 4 in Fig. 14). It dips 45° SE starting near the bending edge of the plate interface at 20–30 km depth. It seems to cut about 40 km deep into the inclined slab and appears like a conjugate fracture pattern of the aftershock sequence of the $M = 6.9$ earthquake of 1999 August 20 (Fig. 11).

In summary, between the NW and SE sections of the investigated area, we observe significant differences in the geometry of the plate interface and in the forearc seismicity patterns. An abrupt structural change occurs between profiles 4 and 5 (Figs 11–13), indicating the transition from the seamount province to the NW rim of the Cocos Ridge connected with the transition to a compressional tectonic regime which is also mentioned in Quintero & Guendel (2000).
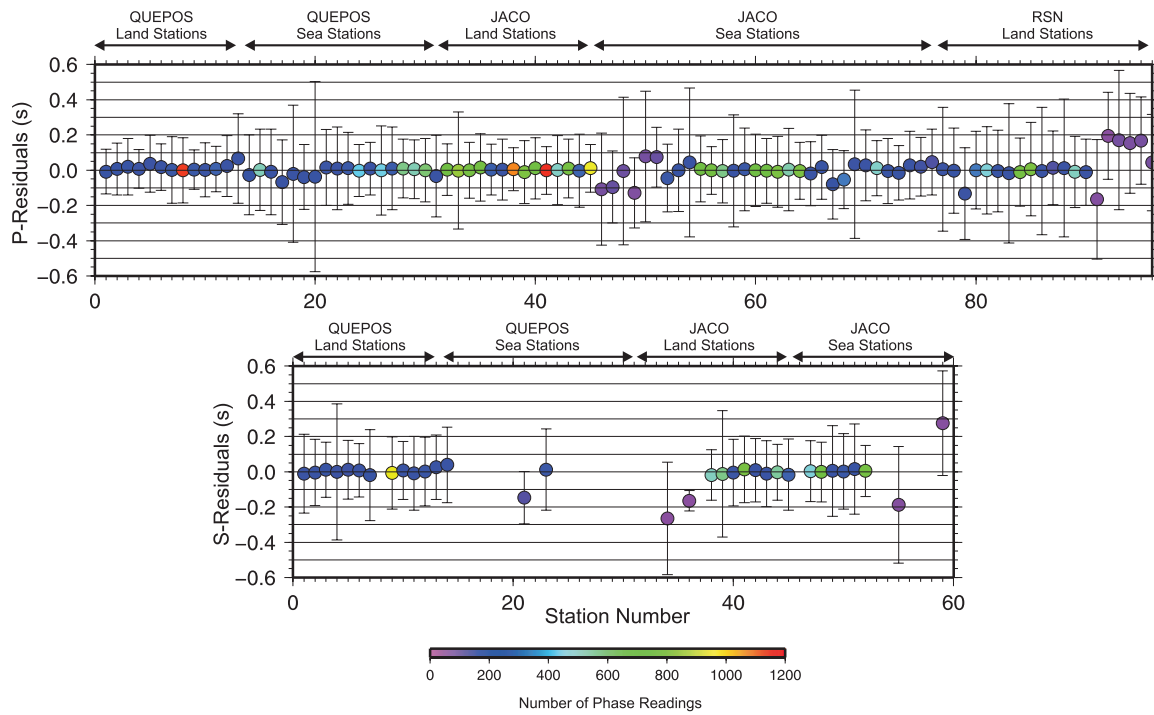
**Figure 9.** Average residual distribution for *P* wave (upper row) and *S* wave (lower row) at each station after the inversion. While *P* waves were recorded at 96 stations, *S* wave were just recorded at 33 stations. Therefore, station number axis for *S* residuals were cut down at the 60th station. Error bars indicate the standard deviation of the residuals. Colours denote the number of phase readings at each station.
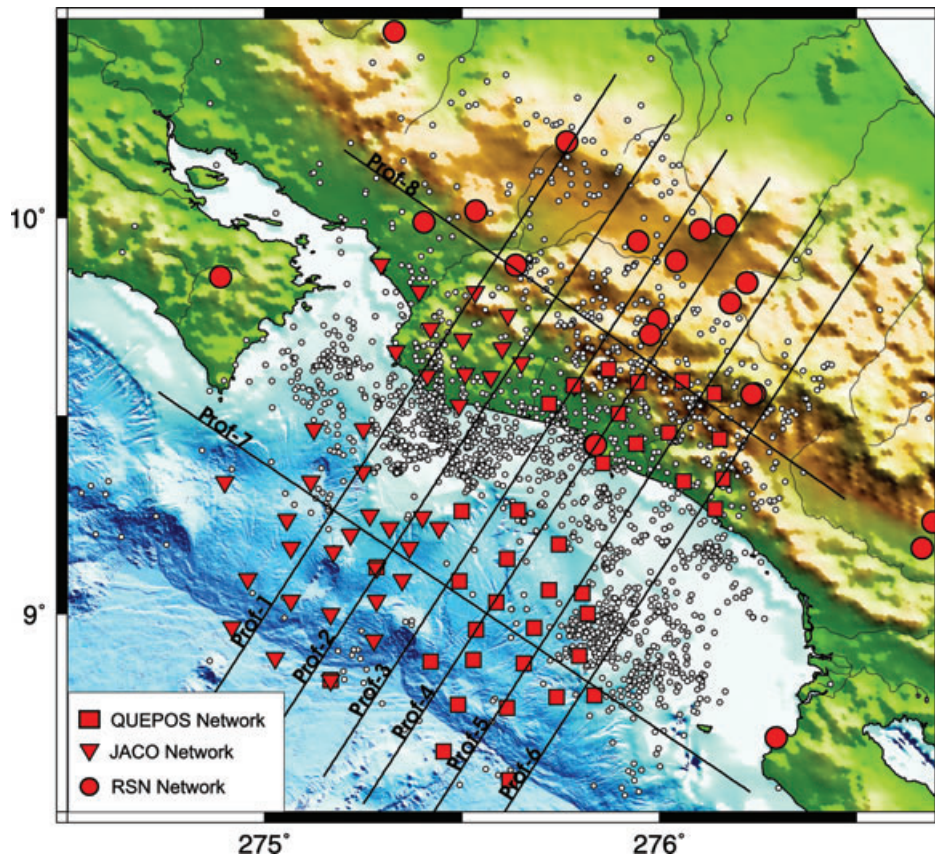


**Figure 10.** Distribution of the accurately located events after local earthquake tomography. The lines show the profiles for vertical sections shown in Figs 11–13. White circles: events recorded from April 2002 to May 2003; red squares: stations of QUEPOS network; red triangles: stations of JACO network; red circles: stations of RSN network.
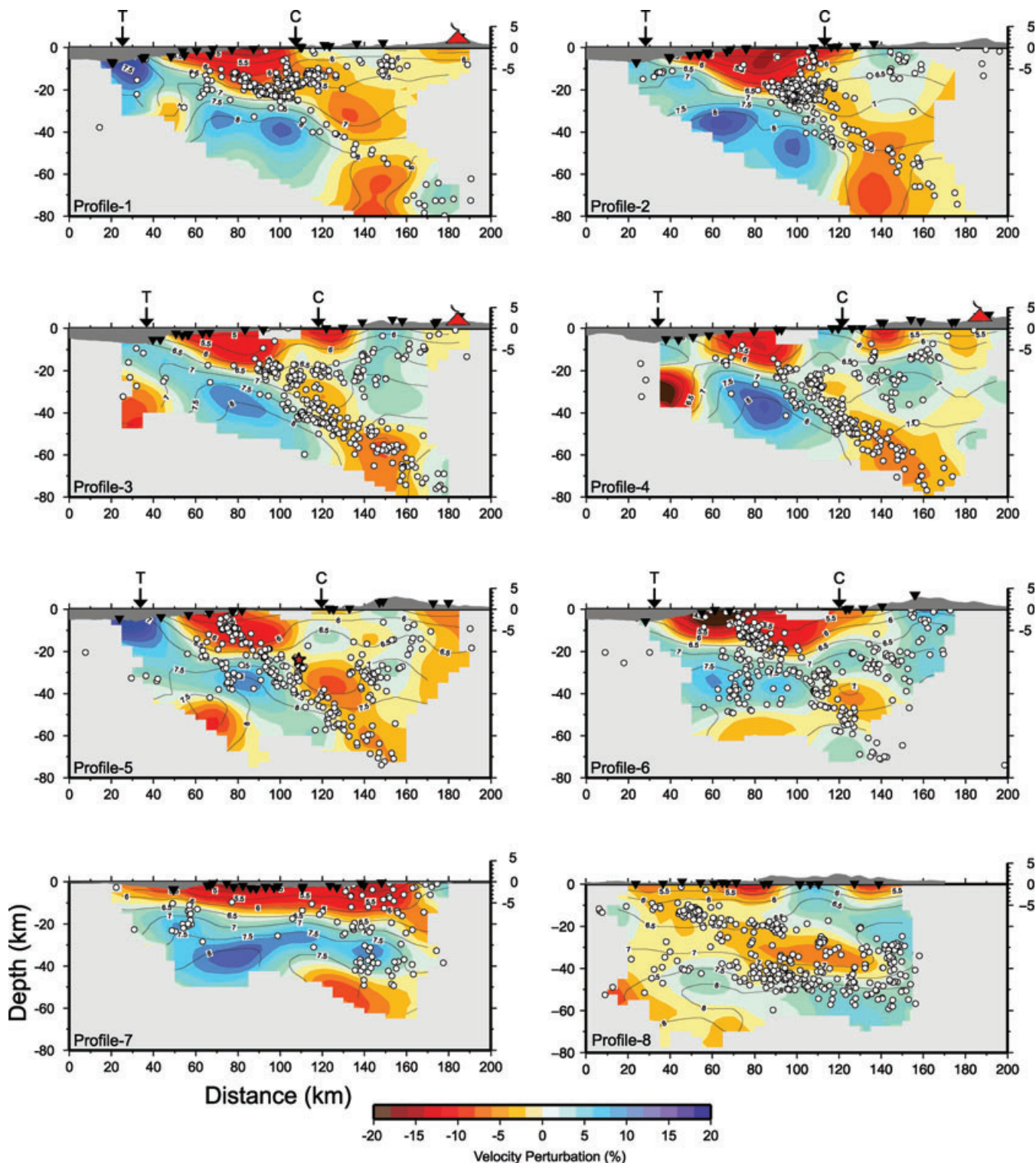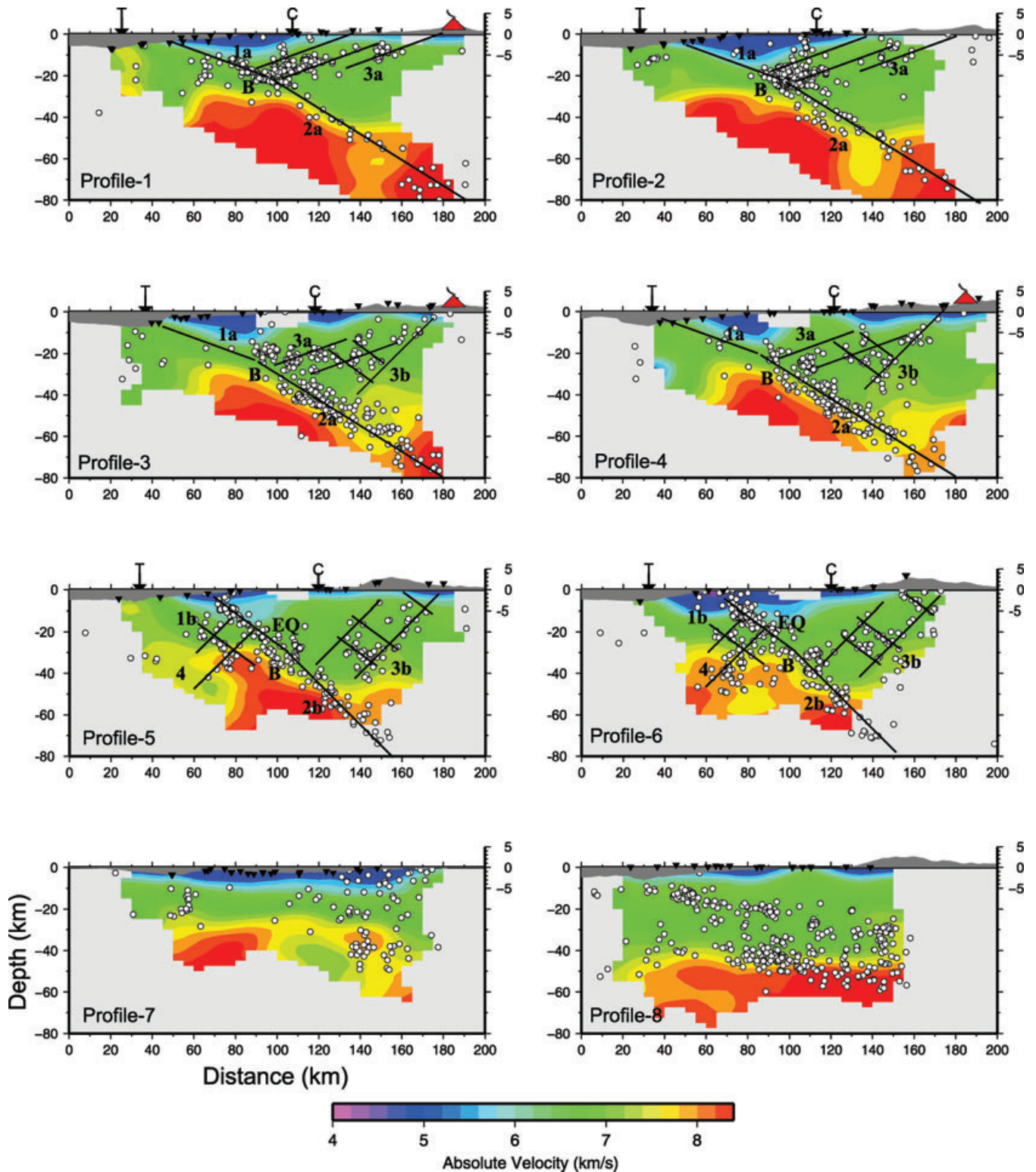
**Figure 11.** Cross-sections of the convergent margin of central Costa Rica showing seismicity and *P*-wave velocity perturbation corresponding to the reference model in Table 1. Location of all cross sections see Fig. 10. Black triangles: seismic stations; white circles: earthquake hypocentres; red triangles: volcanoes; red star indicating 1999 August 20. Quepos earthquake, $M_w = 6.9$; T, trench; C, coast; contour lines indicate absolute *P*-wave velocities with contour interval 0.5 km s$^{-1}$.

## 5.2 Seismic velocity model

Regarding the 3-D seismic velocity models (Figs 11–15), the following findings can be drawn.

(i) The top of the cold subducting Cocos Plate is associated with a positive *P*-wave velocity anomaly of maximum 10 per cent dipping parallel to the WBZ below Costa Rica (Fig. 11). The top of the zone is clearly defined by the upper envelope of the interplate

**Figure 12.** Cross-sections of the convergent margin of Central Costa Rica showing seismicity and corresponding absolute *P*-wave velocities. Location of all cross-sections, see Fig. 10. Black triangles: seismic stations; white circles: earthquake hypocentres; red triangles: volcanoes; T: trench; C: coast. Solid black lines: faults and plate interfaces. 1a,b: seismogenic zone; 2a,b: plate interface at the forearc mantle level; 3a,b: internal deformation zone; 4: oceanic mantle deformation; EQ: hypocentres of aftershocks of the Quepos earthquake (red star in Fig. 11); B: bending point of the downgoing plate and transition to the Wadati–Benioff zone at mantle level. Note that the fault drawings are thought as a tentative interpretation showing the changes visible in the seismicity patterns from N to S. To highlight this change, features 3a (Profile-3) and 3b (Profile-4) are shown for comparison in the respective neighbour profiles, too.
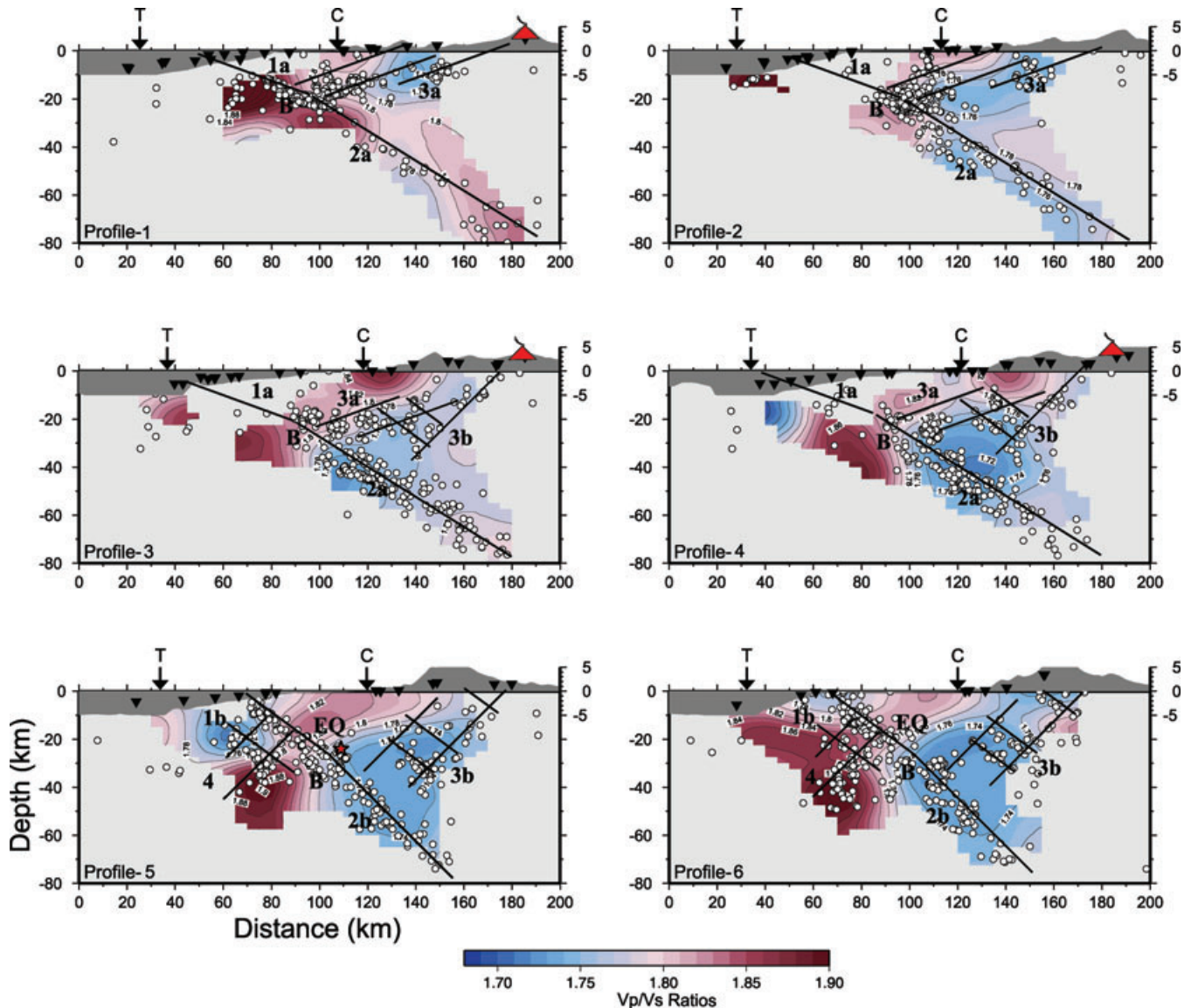
**Figure 13.** Cross-sections through $V_p/V_s$ ratios. Earthquakes (white circles), stations (black triangles), volcanoes (red triangles), trench (T) and coast (C) are projected on to the sections. Profiles are displayed in Fig. 10.

seismicity. In most vertical sections it is connected with a transition from positive to negative velocity found between 5 and −5 per cent with respect to the background model (Table 1). The surface of the high-velocity zone (Fig. 11) is not smooth and shows several step structures. This is particularly evident on profiles 5 and 6 where the step structure seems to be connected with *an extension* of seismicity into the subducting plate (cluster 4; Fig. 14).

(ii) We observe a thickening of the mantle wedge and oceanic crust from northwest to southeast Costa Rica evident from profiles 7 and 8 (Fig. 11), which is parallel to the Middle America Trench. The perturbation of 0 to −5 contour level starts at ∼8 km depth in the north and reaches to ∼20 km depth in the south. This structural change probably reflects the transition from the subducting seamount province to the Cocos Ridge in the south.

(iii) Within the deep crust and upper mantle wedge, an increase in $V_p/V_s$ ratio is found from SE to NW (Figs 13 and 15; depth slices at 30 and 40 km). The transition occurs in the form of a sharp contrast that correlates with the CCRDB (Fig. 1).

(iv) One major feature of the forearc is a zone of low $P$ velocity in the uppermost 10 km between the trench and the coastline (Figs 11 and 12). Because the Costa Rica margin is erosional it can be interpreted as the fractured part of the margin wedge with a high fluid content rather than as an accumulation of sediments. This interpretation is consistent with the observed increase in the $V_p/V_s$ ratio (Fig. 13) and numerous seismic measurements and wide-angle profiles (e.g. von Huene 1995; Hinz *et al.* 1996; Ye *et al.* 1996; von Huene *et al.* 2000).

(v) The deep crust of the overriding plate is characterized by a sequence of basement highs and lows rather than by a layered appearance. This is obvious mainly from the plots of absolute $P$-wave velocity (Fig. 12). The high-velocity lower crust seems to form a tilted block with a sharp velocity transition or discontinuity at about 20 km depth. A comparison with an active seismic profile (Stavenhagen *et al.* 1998) located close to our profile 6 shows that the Moho can be associated most probably with the 7.4 km s$^{-1}$ velocity contour at about 40 km depth.
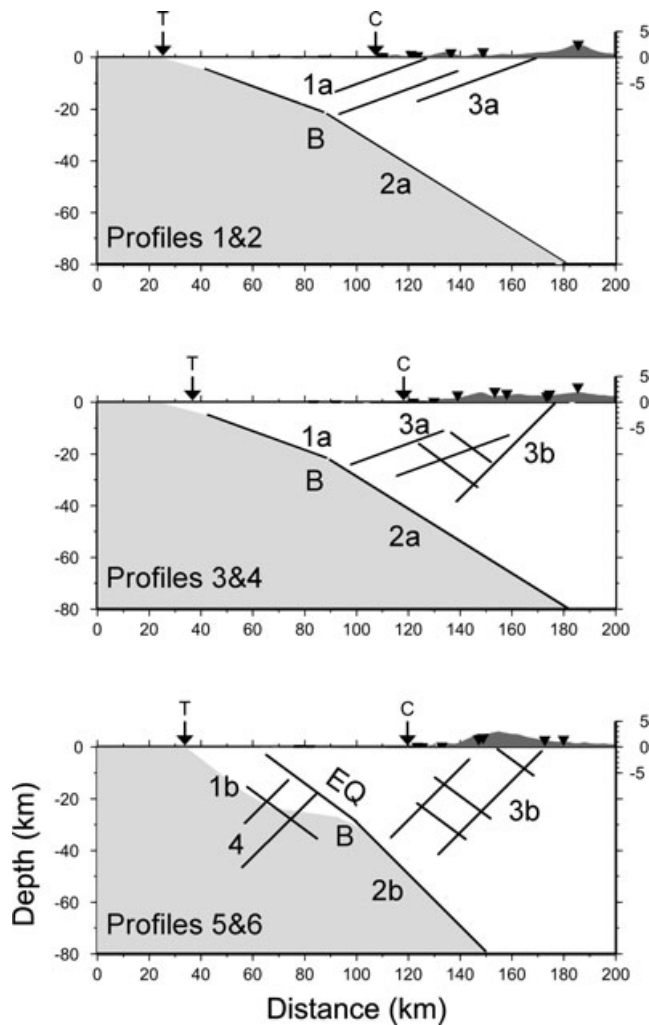
**Figure 14.** A tentative schematic tectonic interpretation based on the seismicity distribution of Figs 11–13. Solid black lines: faults and plate interfaces. 1a,b: seismogenic zone; 2a,b: WBZ; 3a,b: internal deformation zone; 4: oceanic mantle deformation; EQ: hypocentres of aftershocks of the Quepos earthquake (red star in Fig. 11); B: bending point of the downgoing plate and transition to the WBZ.

(vi) Beneath the volcanic arc, the resolution of the tomograms is low. Nevertheless, the results indicate a low *P*-wave velocity anomaly at the Poas and Irazu volcanoes (profiles 1 and 4 in Fig. 11), which can be correlated with the partial melting and upwelling of magma. A corresponding anomaly of the $V_p/V_s$ ratio could not be identified because the *S*-wave velocity structure is not resolved well enough towards the edge of the investigated area.

# 6 DISCUSSION AND CONCLUSION

## 6.1 The seismogenic zone, slab geometry and stress

The seismogenic zone and slab geometry of central Costa Rica exhibit significant spatial variation corresponding to the spatial change of the incoming plate. The general trend shows a steepening of the plate interface towards the south (Fig. 16) and an increasing complexity of the plate contact (Figs 11–16). Our investigation area covers three sections that can be characterized in terms of the geometry of seismicity patterns and *P*-wave velocity structure as follows.

(i) In the northernmost section (profiles 1 and 2 in Figs 11–13), corresponding to the incoming seamount province, the subducting plate interface shows a dip angle of 30° at 20–60 km depth indicated by a sparse homogeneous pattern of earthquakes. In addition, a dense seismicity pattern occurs in the upper overriding plate at depths of less than 25 km. It may be related to the transcurrent fault system of the CCRDB extending through central Costa Rica into the Caribbean Sea. This fault zone is assumed to be caused by the transmission of shear stress coupled into the overriding plate through the rough surface of the subducting plate (Montero 1994; Colombo *et al.* 1997). Generally, profiles 1 and 2 are similar to the findings of DeShon *et al.* (2006) in the area of the Nicoya Peninsula neighbouring in the north.

(ii) The central section (profiles 3 and 4 in Figs 11–13) coincides with the southern part of the CCRDB. The subduction angle and seismicity at the plate interface are still similar to the northern section but a clear change is observed in the spatial distribution of events in the overriding plate. Compared to profiles 1 and 2, where the shallow events seem to follow oblique planes, the geometry of these patterns is less clear. It can possibly be understood as a combination of the patterns found in the north and south sections, indicating a change from extensional stress regime in the north to a highly compressional regime in the south of the central section (Quintero & Guendel 2000).

(iii) The southern section of the investigated area (profiles 5 and 6 in Figs 11–13) is influenced by the subduction of the northern edge of the Cocos Ridge. It differs significantly from the previous sections in both slab geometry and seismicity. In the upper 20 km, the plate interface is nearly horizontal. Between 20 and 60 km depth, the slab gets steeper and again flatter forming a step-shaped cross-section (Fig. 14). Between 40 and 60 km depth, a constant final dip angle of about 45° is observed. In previous studies, only the shallow dip of the upper part of the subducting plate had been recognized and usually interpreted as an underplating feature (Protti *et al.* 1999; Husen *et al.* 2003). Our results show that the situation is probably more complicated: The subduction seems to continue to deeper levels and with a steeper angle than previously thought (Protti *et al.* 1995) and the step-shaped plate interface couples plate motion more intensely than a smooth interface would do. Compared to the northern section, the stress regime is rather collisional style leading to ∼45° dipping conjugate fault planes in the overriding plate. This interpretation is in accordance with the uplift of the Talamanca as such and by the aftershock pattern of the 1999 $M_w = 6.9$ earthquake (EQ in Fig. 12). This aftershock plane terminates approximately at the step-shaped plate interface, at about ∼25 km depth. This coincidence could indicate that this structural heterogeneity of the plate interface may have caused a local stress accumulation later on released in the 1999 earthquake (Bilek *et al.* 2003; DeShon *et al.* 2003).

(iv) The velocity structure of the subducted plate is only weakly constrained by the traveltime data because most hypocentres are located near its surface. Nevertheless, we observe the tendency of a decrease in *P*-wave velocity from northern to southern Costa Rica. This is probably caused by the higher age and lower temperature of the oceanic lithosphere subducting beneath northern Costa Rica. Similar results were obtained by Arroyo *et al.* (2009) to which we refer for a detailed discussion on the possible structure of the subducting slab.

## 6.2 Lateral change in the slab geometry

The lateral change in the slab geometry can be caused by the convergence rate of the incoming plate, the density contrast and thickness
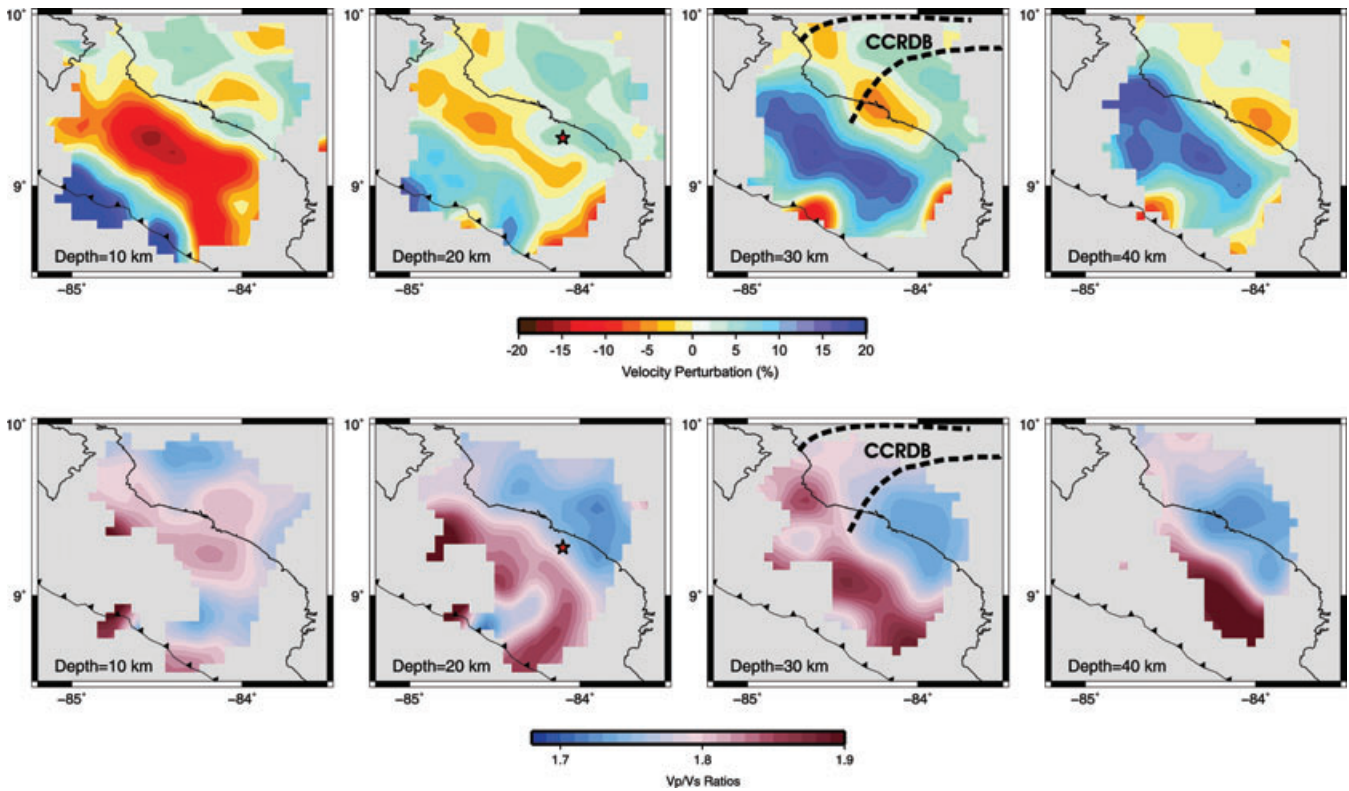
**Figure 15.** Horizontal depth sections of $V_p$ perturbations (upper row) and $V_p/V_s$ ratios (lower row) after the inversion. The reference model (background model) is given in Table 1. $V_p$ perturbations show the lateral variation of the subduction zone. The star indicates the 1999 August 20, $M_w = 6.9$ Quepos earthquake. Location of CCRDB indicated by dashed lines.

of the incoming and overriding plates, pulling forces of the subducted plate portion, friction and deformation in the contact zone. A quantification of these forces in form of a modelling study is beyond the scope of this study, but some aspects can be discussed. The convergence rate of the incoming plate is approximately constant in the investigation area about 9.3 cm yr$^{-1}$ (DeMets 2001). Future modelling of the gravity field will have to show in how far the seismic velocity decrease observed in the incoming plate from north to south is correlated with a density decrease. A density decrease, however, would imply higher buoyancy in the south, which would not be compatible with the observed steepening of the subducting plate interface. Besides age differences, compositional changes of the subducting lithosphere also have to be considered. In the northern segment of our investigation area, the incoming plate shows many seamounts and trench parallel fractures, possibly connected with serpentization, which could lower the density (Ranero *et al.* 2003) and cause uplift in the overriding plate (von Huene *et al.* 2004). The southern section is influenced by the Cocos Ridge with its thickened crust, and it is unclear which of these factors has a stronger effect on local buoyancy. Phase changes related to lateral compositional changes within the slab may also cause lateral variation in slab pull (Zhang & Kayal 2000). However, in summary, plate convergence, buoyancy considerations as well as lateral *P*-wave velocities do not offer an obvious explanation for the dip increase of the plate interface. Rather, the complexity of the *P*-wave velocity model near the plate interface and the seismicity patterns seem to indicate that the dip change could be understood as a consequence of changes in plate coupling and related deformation.

### 6.3 Evidence of fluid transport

The intermediate depth earthquakes of central Costa Rica are supposed to be triggered by dehydration (Hacker *et al.* 2003; Husen *et al.* 2003). Husen *et al.* (2003) calculated the predicted dehydration depth of hydrous minerals depending on Hacker *et al.* (2003) from onshore central Costa Rica, along a profile close to the profile-2 (Fig. 11) of this study. Most of the mineral dehydration depths correspond well to the distribution of the intermediate depth earthquakes. *P*-wave tomography shows a low-velocity zone in the mantle wedge at about 40 km depth (profiles 1–3 in Fig. 11), which would correspond to a very low local mantle $V_p$ (about 7.2–7.4 km s$^{-1}$) possibly indicating hydration of the mantle wedge. The *P*-wave velocity is lower on profiles 1–3 (Figs 11 and 12) than on profiles 4–6 (Figs 11 and 12), indicating that the fluid input into the mantle wedge is higher in the fractured seamount province than in Cocos Ridge area. Further evidence of fluid transport through the crust may be seen in the seismicity patterns connecting the plate interface to the forearc and arc along profile 1–3 (pattern type 3a in Fig. 14). These patterns may represent a fault system through which fluids released from subducted rocks can rise up to the volcanic arc.

### 6.4 Central Costa Rica deformation belt: edge of the volcanic arc

The active part of the Costa Rican volcanic arc terminates at the CCRDB. Beneath the CCRDB, we find a significant contrast in
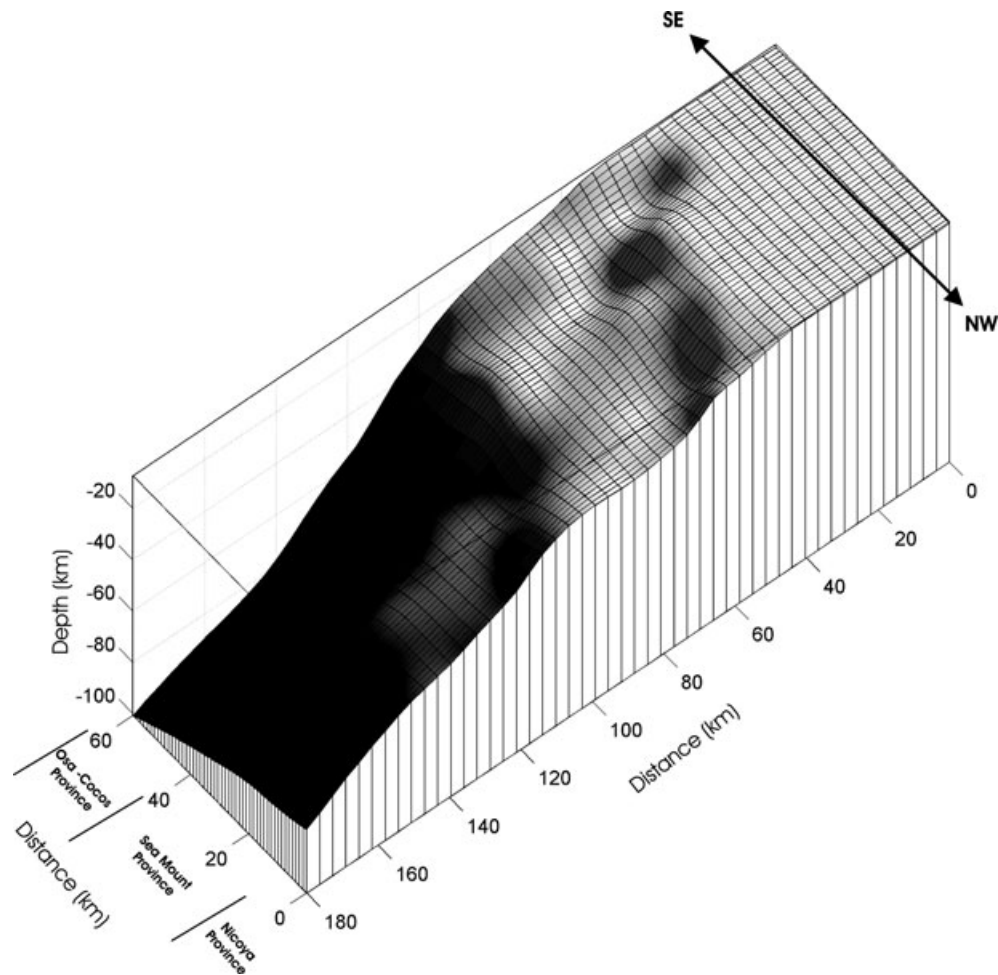
**Figure 16.** Flying carpet showing the lateral structural changes. Zero perturbation contour which is almost the upper envelope of the slab are digitized from all the vertical sections (Fig. 10) perpendicular to the MAT. The data in between is interpolated by MATLAB 4 griddata method.

*P*-wave velocity and $V_p/V_s$ ratio reaching down to 40 km depth (Fig. 15). Therefore, the CCRDB, separating the northwestern and southeastern parts of Costa Rica, can be interpreted as a major crustal transition zone connected also with the beginning gap of the volcanic chain in the south. Again, this transition zone can be understood as the result of the changing structure of the incoming plate with the fractured dewatering seamount province in the NW and the Cocos Ridge in the SE causing a thickening of the overriding plate and transferring a smaller amount of water into the mantle wedge beneath the Talamanca. Beneath the active part of the volcanic arc, an increased $V_p/V_s$ ratio of 1.8 is found at 30 km depth (Fig. 13). Most of the crustal earthquakes are found in the transition zone from high to low $V_p/V_s$ values attributed to the CCRDB, which, therefore, has to be regarded as a highly deformed region down to depths of 30 km.

## ACKNOWLEDGMENTS

## REFERENCES

Arroyo, I.G., Husen, S., Flueh, E.R., Gossler, J., Kissling, E. & Alvarado, G.E., 2009. Three-dimensional P-wave velocity structure on the shallow part of the Central Costa Rican Pacific margin from local earthquake tomography using off- and onshore networks, *Geophys. J. Int.,* **179,** 827–849.

Barckhausen, U., Ranero, C.R., vonHuene, R., Cande, S.C. & Roeser, H.A., 2001. Revised tectonic boundaries in the Cocos Plate off Costa Rica: implications for the segmentation of the convergent margin and for plate tectonic models, *J. geophys. Res.,* **106,** 19 207–19 220.

Bialas, J. & Flueh, E.R., 1999. Ocean bottom seismometers, *Sea Technol.,* **40,** 41–46.

Bilek, S.L., Schwarz, S.Y. & DeShon, H.R., 2003. Control of seafloor roughness on earthquake rupture behavior, *Geology,* **31,** 455–458.

Bundschuh, J. & Alvarado, G. A., 2007. *Central America: Geology, Resources and Hazards,* Taylor & Francis, London.

Carr, M., Feigenson, M.D., Patino, L.C. & Walker, J.A., 2003. Volcanism and geochemistry in Central America: progress and problems, *Geophys. Monogr.,* **138,** 153–174.

Carr, M.J. *et al*., 2007. Element fluxes from the volcanic front of Nicaragua and Costa Rica, *Geochem. Geophys. Geosci.,* **8,** 1–22.

Colombo, D., Cimini, G.B. & de Franco, R., 1997. Three dimensional velocity structure of the upper mantle beneath Costa Rica from teleseismic tomography study, *Geophys. J. Int.,* **131,** 189–208.

DeMets, C., 2001. A new estimate for present-day Cocos-Caribbean plate motion: implications for slip along the Central American volcanic arc, *Geophys. Res. Lett.,* **28,** 4043–4046.

DeShon, H.R., Schwartz, S.Y., Bilek, S.L., Dorman, L.M., Gonzalez, V., Protti, J.M., Flueh, E.R. & Dixon, T.H., 2003. Seismogenic zone structure of the southern Middle America Trench, Costa Rica, *J. geophys. Res.,* **108,** 2491.

DeShon, H.R. *et al.,* 2006. Seismogenic zone structure beneath the Nicoya Peninsula, Costa Rica, from three-dimensional local earthquake P- and S-wave tomography, *Geophys. J. Int.,* **164,** 109–124.

Flueh, E.R. & von Huene, R., 2007. Crustal structure, in *Central America: Geology, Resources and Hazards,* pp. 267–274, eds Bunddchuh, J. & Alvarado, G., Taylor & Francis, London.

Gardner, T.W. & Verdonck, D. & Pinter, N.M., 1992. Quaternary uplift astride the aseismic Cocos Ridge, Pacific coast, Costa Rica, *GSA Bull.,* **104,** 219–232.

Graefe, K., 1998. Exhumation and thermal evolution of the Cordillera de Talamanca (Costa Rica): constraints from fission track analysis, 40Ar-39Ar and 87Rb-87Sr chronology, *PhD thesis.* Universität Tübingen, Germany.

Hacker, B.R., Peacock, S.M., Abers, G.A. & Holloway, S.D., 2003. Subduction factory 2. Are intermediate-depth earthquakes in subducting slabs linked to metamorphic dehydration reactions? *J. geophys. Res.,* **108,** 2030, doi:10.1029/2001JB001129.

Hauff, F., Hoernle, K., Schmincke, H.U. & Werner, R., 1997. A Mid Cretaceous origin for the Galapagos hotspot: volcanological, petrological and geochemical evidence from Costa Rican oceanic crustal segments, *Int. J. Earth Sci.,* **86,** 141–155.

Hinz, K., von Huene, R. & Ranero, C.R., 1996. Tectonic structure of the convergent Pacific margin offshore Costa Rica from multichannel seismic reflection data, *Tectonics,* **15,** 54–66.

Hoernle, K. & Hauff, F., 2007. Oceanic igneous complexes in Central America, in *Central America: Geology, Resources and Hazards,* pp. 523–548, ed. Bunddchuh, J. & Alvarado, G., Taylor & Francis, London.

Husen, S., Kissling, E. & Quintero, R., 2002. Tomographic evidence for a subducted seamount beneath the Gulf of Nicoya, Costa Rica: the cause of the 1990 Mw = 7.0 Gulf of Nicoya earthquake, *Geophys. Res. Lett.,* **29,** 79–71.

Husen, S., Quintero, R., Kissling, E. & Hacker, B., 2003. Subduction-zone structure and magmatic processes beneath Costa Rica constrained by local earthquake tomography and petrological modelling, *Geophys. J. Int.,* **155,** 11–32.

Kissling, E., Ellsworth, W., Eberhart-Phillips, D. & Kradolfer, U. 1994. Initial reference models in local earthquake tomography, *J. geophys. Res.,* **99,** 19 635–19 646.

Koulakov, I. *et al.,* 2007. P and S velocity structure of the crust and the upper mantle beneath central Java from local tomography inversion, *J. geophys. Res.,* **112,** 8310, doi:10.1029/2006JB004712.

Koulakov I., 2009a. LOTOS code for local earthquake tomographic inversion. Benchmarks for testing tomographic algorithms, *Bull. seism. Soc. Am.,* **99**(1), 194–214, doi:10.1785/0120080013.

Koulakov I., 2009b. Out-of-network events can be of great importance for improving results of local earthquake tomography, *Bull. seism. Soc. Am.,* **99**(4), 2556–2563, doi:10.1785/0120080365.

Montero, W., 1994. Neotectonics and related stress distribution in a subduction-collisional zone: Costa Rica, in *Geology of an Evolving Island Arc: The Isthmus of Southern Nicaragua, Costa Rica and Western Panama, Profil,* Vol. 7, pp. 126–141, eds Seyfried, H. & Hellmann, W., Universität Stuttgart.

Newman, A.V., Schwartz, S.Y., Gonzalez, V., DeShon, H.R., Protti, J.M., & Dorman, L.M., 2002. Along-strike variability in the seismogenic zone below Nicoya Peninsula, Costa Rica, *Geophys. Res. Lett.,* **29,** 38–31.

Norabuena, E. *et al.,* 2004. Geodetic and seismic constraints on some seismogenic zone processes in Costa Rica, *J. geophys. Res.,* **109,** 11 403, doi:10.1029/2003JB002931.

Paige, C.C. & Saunders, M.A., 1982. LSQR: an algorithm for sparse linear equations and sparse least squares, *ACM Trans. Math. Software,* **8,** 43–71.

Protti, M., Guendel, F. & McNally, K., 1994. The geometry of the Wadati-Benioff zone under southern Central America and its tectonic signifi-cance: results from a high-resolution local seismographic network, *Phys. Earth planet. Inter.,* **84,** 271–287.

Protti, M., Guendel, F. & McNally, K., 1995. Correlation between the age of the subducting Cocos plate and geometry of the Wadati-Benioff zone under Nicaragua and Costa Rica, *Geol. Soc. Am. Spec. Paper,* **295,** 309–326.

Protti, M., Schwartz, S.Y. & Zandt, G., 1999. Simultaneous inversion for earthquake location and velocity structure beneath central Costa Rica, *Bull. seism. Soc. Am.,* **86,** 19–31.

Quintero, R. & Guendel, F., 2000. Stress field in Costa Rica, Central America, *J. Seismol.,* **4,** 297–319.

Quintero, R. & Kissling, E., 2001. An improved P-wave velocity reference model for Costa Rica, *Geofis. Int.,* **40,** 3–19.

Rafael, B.P. & Alvaro, C.M., 1999. in Los Temblores de la zona de Quepos de agosto de 1999, fuente seismica características tectónicas, pp. 1–13, Instituto Costarricense de Electricidad, Proyectos y Servicios Asociados Exploración Subterranea.

Ranero, C.R., Phipps, M.J., McIntosh, K. & Reichert, C., 2003. Bending-related faulting and mantle serpentinization at the Middle America Trench, *Nature,* **425,** 367–373.

Sallares, V. & Charvis, P., 2003. Crustal thickness constraints on the geodynamic evolution of the Galapagos Volcanic Province, *Earth planet. Sci. Lett.,* **214,** 545–559.

Sallares, V., Danobeitia, J.J. & Flueh, E.R., 2000. Seismic tomography with local earthquakes in Costa Rica, *Tectonophysics,* **296,** 61–78.

Sallares, V., Charvis, P., Flueh, E.R. & Bialas, J., 2005. Seismic structure of the Carnegie ridge and the nature of the Galapagos hotspot, *Geophys. J. Int.,* **161,** 763–788.

Stavenhagen, A.U., Flueh, E.R., Ranero, C., McIntosh, K.D., Shipley, T., Leandro, G., Schultze, A. & Danobeitia, J.J., 1998, Seismic wide-angle investigations in Costa Rica—A crustal velocity model from the Pacific to the Caribbean, *Zentralbl. Geol. Palaeontol., Teil 1,* **3**(6), 393–408

Um, J. & Thurber, C., 1987. A fast algorithm for two point seismic ray tracing, *Bull. seism. Soc. Am.,* **77,** 972–986.

Van Der Sluis, A. & van der Vorst, H.A., 1987. Numerical solution of large, sparse linear algebric systems arising from tomographic problems, in *Seismic Tomography,* pp. 49–83, ed. Nolet, G., Reidel, Dordrecht.

von Huene, R., Ranero, C.R., Weinrebe, W. & Hinz, K., 2000. Quaternary convergent margin tectonics of Costa Rica, segmentation of the Cocos Plate, and central American volcanism, *Tectonics,* **19,** 314–334.

von Huene, R., Ranero, C.R. & Watts, P., 2004. Tsunamigenic slope failure along the Middle America Trench in two tectonic settings, *Marine Geol.,* **203,** 303–317.

von Huene, R.E.A., 1995. Morphotectonics of the Pacific convergent margin of Costa Rica, *Geol. Soc. Am. Spec. Paper,* **295,** 291–307.

Walther, C. & Flueh, E.R., 2002. Remnant of the ancient Farallon Plate breakup: a low-velocity body in the lower oceanic crust off Nicoya Peninsula, Costa Rica—evidence from wide-angle seismics, *Geophys. Res. Lett.,* **29,** 45–41.

Walther, C.H.E., 2003. The crustal structure of the Cocos Ridge off Costa Rica, *J. geophys. Res.,* **108,** 2136, doi:10.1029/2001JB000888.

Walther, C.H.E., Flueh, E.R., Ranero, C.R., von Huene, R. & Strauch, W., 2000. Crustal structure across the Pacific margin of Nicaragua: evidence for ophiolitic basement and a shallow mantle sliver, *Geophys. J. Int.,* **141,** 759–777.

Werner, R., Hoernle, K., Van Den Bogaard, P., Ranero, C., von Huene, R. & Korich, D., 1999. Drowned 14-m.y.-old Galapagos archipelago off the coast of Costa Rica: implications for tectonic and evolutionary models, *Geology,* **27,** 499–502.

Wilson, D.S., Teagle, D.A. & Acton, G.D., 2003. First results from hole 1256D—a new ocean-crust reference hole drilled in fast-spread crust during ODP Leg 206, *AGU Fall Meeting Abstracts,* pp. A2.

Yao, Z.S., Quintero, R. & Roberts, R.G., 1999. Tomographic imaging of P- and S-wave velocity structure beneath Costa Rica, *J. Seism.,* **3,** 177–190.

Ye, S., Bialas, J., Flueh, E.R., Stavenhagen, A., von Huene, R., Leandro, G. & Hinz, K., 1996. Crustal structure of the Middle American Trench off Costa Rica from wide-angle seismic data, *Tectonics,* **15,** 1006–1021.

Zhang, H. & Kayal, J.R., 2000. Impact of seismic tomography, *Science,* **79,** 1208–1214.